Applied Surface Science 329 (2015) 143–149

Contents lists available at ScienceDirect

Applied Surface Science

journal homepage: www.elsevier.com/locate/apsusc

Enhanced visible-light photoactivity of g-C_3N_4 via Zn_2SnO_4 modification

Lihong Zhang [a], Xiaoxing Wang [a], Qingyan Nong [a], Hongjun Lin [c], Botao Teng [b], Yuting Zhang [a], Leihong Zhao [b], Tinghua Wu [b], Yiming He [a,*]

[a] *Department of Materials Physics, Zhejiang Normal University, Jinhua 321004, China*
[b] *Institute of Physical Chemistry, Zhejiang Normal University, Jinhua 321004, China*
[c] *College of Chemistry and Life Sciences, Zhejiang Normal University, Jinhua 321004, China*

ARTICLE INFO

Article history:
Received 19 July 2014
Received in revised form
27 November 2014
Accepted 22 December 2014
Available online 30 December 2014

Keywords:
Photocatalysis
g-C_3N_4
Zn_2SnO_4
Visible light

ABSTRACT

The objective of this research was to prepare, characterize and evaluate the photocatalytic activity of Zn_2SnO_4/g-C_3N_4 composite in RhB degradation under visible light irradiation. The composite was synthesized by simple calcination of Zn_2SnO_4–melamine mixture, and was characterized by various techniques including Brunauer–Emmett–Teller method (BET), X-ray diffraction (XRD), scanning electron microscopy (SEM), transmission electron microscopy (TEM), X-ray photoelectron spectroscopy (XPS), UV–vis diffuse reflectance spectroscopy (DRS), and photoluminescence spectroscopy (PL). Characterization results indicated that the decoration of Zn_2SnO_4 on g-C_3N_4 showed nearly no effect on its light absorption performance, but promoted the surface area of the composite, which benefited the adsorption of dyes and the subsequent photocatalytic process. However, more significant was the formation of hetero-junction structure between Zn_2SnO_4 and g-C_3N_4, which efficiently promoted the separation of electron–hole pairs and enhanced the photocatalytic performance of Zn_2SnO_4/g-C_3N_4. The optimal Zn_2SnO_4/g-C_3N_4 photocatalyst showed a degradation rate of 0.038 min^{-1}, which was 3.2 times higher than that of g-C_3N_4. In addition, the Zn_2SnO_4/g-C_3N_4 composite shows high stability. $^{\bullet}O_2^-$ and h^+ were the main reactive species.

1. Introduction

Visible-light-driven heterogeneous photocatalysis has been widely recognized as a potential strategy for solar energy conversion and environmental remediation. Great efforts have been made to develop an efficient photocatalyst under visible light. Of the well-known semiconductor photocatalysts, graphitic carbon nitride (g-C_3N_4), a polymeric metal-free semiconductor with a band gap of about 2.70 eV, has been recently focused due to its high stability, low cost and response to visible-light [1]. However, currently, the activity of g-C_3N_4 in photocatalytic reaction is not high. More and more researchers recognized that pure g-C_3N_4 was hardly competent for efficient solar conversion due to the disadvantages of limited visible-light harvesting and rapid charge recombination. Therefore, a variety of semiconductors, such as MoO_3 [2], $SmVO_4$ [3], MoS_2 [4], and AgX (X = Br, I) [5], have been doped on g-C_3N_4 to promote the photoactivity by forming hetero-junction structures. Scientists normally use visible-light-responsive semiconductors as the dopers. This kind of semiconductor was believed to promote the photoactivity of g-C_3N_4 more efficiently than that with a wide band gap, since the former can improve the catalyst's abilities in both light adsorption and charge separation. However, our previous work indicated that the rule resulted from the research of TiO_2 was not suitable for the g-C_3N_4 based composite photocatalyst [6]. The semiconductor with a wide band gap can also promote the photocatalytic activity of g-C_3N_4 efficiently. For example, both Wang and Liu synthesized a g-C_3N_4 photocatalyst hybridized with ZnO using a milling-heat treatment method [7,8]. The synthesized ZnO/g-C_3N_4 composite showed much higher photocatalytic activity than pure g-C_3N_4 in MO degradation under visible light irradiation. Pan et al. reported that the decoration of $BiPO_4$ on g-C_3N_4 dramatically promoted the reaction rate of methyl blue degradation from 0.06 to 0.31 h^{-1} [9]. The promotion effect of $BiPO_4$ was even higher than those of many visible-light-driven semiconductors, including TaON, $DyVO_4$ and $BiVO_4$ [10–12].

Zinc stannate (Zn_2SnO_4) is an n-type transparent conducting oxide with a wide band gap of 3.35 eV [13]. It is a very important material in various areas, such as gas sensor,

---

* Corresponding author. Tel.: +86 0579 83792294; fax: +86 0579 83714946.
E-mail address: hym@zjnu.cn (Y. He).

http://dx.doi.org/10.1016/j.apsusc.2014.12.154
0169-4332/© 2014 Elsevier B.V. All rights reserved.

negative electrode material for Li-ion battery, and synergistic flame retardants [13–17]. In addition, it has also attracted considerable interest for its high photocatalytic activity under UV light. The decomposition reactions of benzene and water-soluble dyes using Zn_2SnO_4 as a photocatalyst were reported [18,19]. To the best of our knowledge, however, no research focused on the promotion effect of Zn_2SnO_4 on the photocatalytic activity of g-C_3N_4 has been reported. Hence, in this paper, we present the first example of a Zn_2SnO_4–hybridized g-C_3N_4 photocatalyst prepared by a simple mixing-calcination method. The photocatalytic testing result indicated that the photocatalytic activity of g-C_3N_4 for RhB photodegradation was enhanced effectively after the hybridization with the Zn_2SnO_4.

2. Experimental

2.1. Catalysts preparation

All chemicals were analytical pure reagent and purchased commercially without further purification. Pure g-C_3N_4 was prepared by directly heating melamine at 520 °C in a muffle furnace for 4 h in at a heating rate of 10 °C/min. The preparation of Zn_2SnO_4 refers to the previous literature [20]. Typically, 2.5 mmol zinc chloride and 1.25 mmol tin (IV) chloride pentahydrate were dissolved in mixture of 20 mL water and 20 mL ethanol. Then, 10 mL of 1.0 M NaOH aqueous solution was added dropwise. After stirring for 15 min, the obtained slurry was transferred to a 100 mL Teflon-lined autoclave, and then kept in an oven at 200 °C for 24 h. The precipitates were washed several times and then dried to obtain white Zn_2SnO_4 powders.

The Zn_2SnO_4/g-C_3N_4 composites were prepared as follows: a series different amounts of Zn_2SnO_4 with a suitable amount of melamine were added into a motor and then grounded for 30 min. The resultant mixed powder was put into a crucible with a cover and then heated at 520 °C in a muffle furnace for 4 h to obtain Zn_2SnO_4/g-C_3N_4 hybrids with various Zn_2SnO_4 contents. Thermogravimetric analysis (TG) was used to determine the weight contents of Zn_2SnO_4 in the composite. Based on the characterization results (Fig. S1), the Zn_2SnO_4/g-C_3N_4 composites with different Zn_2SnO_4 concentrations were named as 5.4 wt.% ZSC, 10.4 wt.% ZSC, 13.7 wt.% ZSC and 20.9 wt.% ZSC, respectively.

2.2. Characterizations

TG analysis (Netzsch STA449) was carried out in a flow of air (20 mL/min) at a heating rate of 10 °C/min. BET surface areas were measured from N_2 sorption–desorption isotherms at 77 K using an Autosorb-1 apparatus (Quantachrome Instruments). XRD measurement was carried out on a Philips PW3040/60 using Cu Kα radiation. SEM and TEM images were taken on a field emission scanning electron microscope (Nanoscope IIIa) and a Hitachi S-4800 transmission electron microscope, respectively. DRS measurements were performed on a UV–vis spectrometer (Thermo Nicolet Evolution 500) using $BaSO_4$ as a reference sample. XPS spectra were obtained by using a Quantum 2000 Scanning ESCA Microprobe instrument using Al Kα. PL spectra were recorded on a FLS-920 spectrometer (Edinburgh Instrument), using a Xe lamp (excitation at 365 nm) as light source. Electrochemical impedance spectroscopy (EIS) and photoelectric current (PC) responses measurements were performed using a CHI 660B electrochemical workstation with a standard three-electrode cell at room temperature.

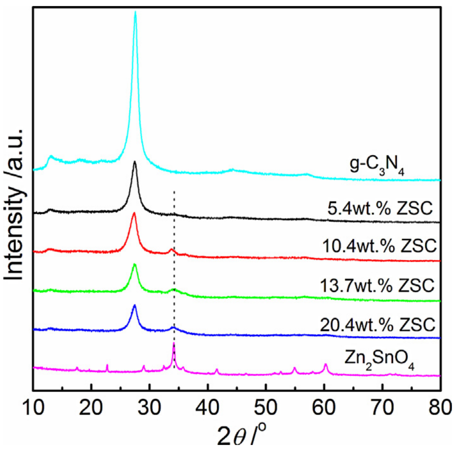

Fig. 1. XRD patterns of Zn_2SnO_4/g-C_3N_4 composites with different Zn_2SnO_4 concentrations.

2.3. Photocatalyic reaction

The photocatalytic activities of $ZnSnO_4$/g-C_3N_4 hybrids were tested by degradation of 100 mL rhodamine B (RhB, 10 mg/L) in a photoreaction apparatus under visible-light irradiation. Visible light ($420 < \lambda < 800$ nm) was generated by a 350 W Xe lamp equipped with two optical filters. The catalyst content was 0.2 g/100 mL. Prior to irradiation, the suspensions were magnetically stirred in dark for 60 min to reach the adsorption–desorption equilibrium. During the RhB photodecomposition, samples were withdrawn at regular intervals and centrifuged to separate solid particles for analysis. The concentration of the RhB was determined by a UV–vis spectroscopy at its maximum absorption wavelength. The examination experiment of reactive species is similar to the photodegradation experiment. A quantity of scavengers was introduced into the RhB solution prior to addition of the catalyst. The concentration of scavengers was controlled to be 0.01 mol/L according to the previous studies [21,22].

3. Results and discussion

3.1. Characterizations of Zn_2SnO_4/g-C_3N_4 composites

The BET surface area of g-C_3N_4 is 9.0 m^2/g which is much smaller than that of Zn_2SnO_4 (40.7 m^2/g). The addition of Zn_2SnO_4 increases the surface area. The BET surface area of 5.4 wt.% ZSC, 10.4 wt.% ZSC, 13.7 wt.% ZSC and 20.4 wt.% ZSC samples are 11.5, 12.0, 15.0 and 22.8 m^2/g, respectively.

The powder XRD patterns of g-C_3N_4, Zn_2SnO_4, and the Zn_2SnO_4/g-C_3N_4 composites are shown in Fig. 1. Two pronounced peaks are found in g-C_3N_4 at 27.4 and 13.0°, which can be indexed to (0 0 2) and (0 0 1) diffraction planes of the graphite-like carbon nitride [1]. For Zn_2SnO_4, several peaks at 17.5, 22.7, 29.0, 32.5, 34.2, 35.7, 41.5, 52.5, 54.9 and 60.3° are observed, indicating its cubic phase (JCPDS No. 24-1470). The Zn_2SnO_4/g-C_3N_4 sample presents a two phase composition: Zn_2SnO_4 and g-C_3N_4. With the increase of Zn_2SnO_4 concentration, the XRD peaks of Zn_2SnO_4 strengthen at the expense of those of g-C_3N_4.

Fig. 2 shows the morphology of g-C_3N_4, Zn_2SnO_4 and 10.4 wt.% ZSC characterized by SEM and TEM. Pure g-C_3N_4 exhibits an aggregation of wrinkled sheets, which is different from Zn_2SnO_4 nanoparticles. In the SEM image of Zn_2SnO_4/g-C_3N_4, both the two materials are observed. The small particles of Zn_2SnO_4 are anchored on g-C_3N_4 surface, indicating the hybrid structure of Zn_2SnO_4/g-C_3N_4. This structure is further proven by the TEM image (Fig. 2d) since Zn_2SnO_4 is darker than g-C_3N_4. Meanwhile, given that the